ADVANCES IN ATMOSPHERIC SCIENCES, VOL. 26, NO. 3, 2009, 480–492

The East Asia-Western North Pacific Boreal Summer Intraseasonal Oscillation Simulated in GAMIL 1.1.1

YANG Jing*[1,2] (杨 静), Bin WANG[3], WANG Bin[1] (王 斌), and LI Lijuan[1] (李立娟)

[1]*State Key Laboratory of Numerical Modeling for Atmospheric Sciences and Geophysical Fluid Dynamics, Institute of Atmospheric Physics, Chinese Academy of Sciences, Beijing* 100029

[2]*State Key Laboratory of Earth Surface Processes and Resource Ecology, Beijing Normal University, Beijing* 100875

[3]*Department of Meteorology and International Pacific Research Center, University of Hawaii at Manoa, Honolulu, HI* 96822*, USA*

(Received 8 May 2008; revised 30 June 2008)

ABSTRACT

We evaluate the performance of GAMIL1.1.1 in a 27-year forced simulation of the summer intraseasonal oscillation (ISO) over East Asia (EA)-western North Pacific (WNP). The assessment is based on two measures: climatological ISO (CISO) and transient ISO (TISO). CISO is the ISO component that is phase-locked to the annual cycle and describes seasonal march. TISO is the ISO component that varies year by year.

The model reasonably captures many observed features of the ISO, including the stepwise northward advance of the rain belt of CISO, the dominant periodicities of TISO in both the South China Sea-Philippine Sea (SCS-PS) and the Yangtze River Basin (YRB), the northward propagation of 30–50-day TISO and the westward propagation of the 12–25-day TISO mode over the SCS-PS, and the zonal propagating features of three major TISO modes over the YRB. However, the model has notable deficiencies. These include the early onset of the South China Sea monsoon associated with CISO, too fast northward propagation of CISO from 20°N to 40°N and the absence of the CISO signal south of 10°N, the deficient eastward propagation of the 30–50-day TISO mode and the absence of a southward propagation in the YRB TISO modes.

The authors found that the deficiencies in the ISO simulation are closely related to the model's biases in the mean states, suggesting that the improvement of the model mean state is crucial for realistic simulation of the intraseasonal variation.

Key words: intraseasonal oscillation (ISO), East Asia-Western North Pacific (EA-WNP)

Citation: Yang, J., B. Wang, B. Wang, and L. J. Li, 2009: The East Asia-western North Pacific boreal summer intraseasonal oscillation simulated in GAMIL 1.1.1. *Adv. Atmos. Sci.*, **26**(3), 480–492, doi: 10.1007/s00376-009-0480-7.

1. Introduction

The prediction of intraseasonal oscillation (ISO) can fill the gap between weather forecast and climate prediction, and is an indispensable portion of the seamless forecast. Evaluation of the model's ISO is a necessary step towards the improvement of intraseasonal prediction. A majority of the evaluation of ISO has been focused on Madden Julian Oscillation (MJO, Madden and Julian, 1971) (e.g., Slingo and Madden, 1991; Slingo et al., 1996; Sperber, 2004; Lin et al., 2006). Prominent shortcomings highlighted in the above MJO modeling studies include higher phase speeds, shorter periods and smaller amplitudes. The uncertainties in the interactive physical parameterizations and the deficiencies to capture multi-scale interaction are considered to be major hurdles for the realistic simulation of the MJO (e.g., Chao and Deng,

*Corresponding author: YANG Jing, yangjing@bnu.edu.cn

1998; Lee et al., 2003; Liu et al., 2005; Wang, 2005).

Compared with the MJO simulation, the boreal summer ISO simulation in the Asian monsoon region is a more challenging task. This is primarily due to its multi-periodicity (e.g., Krishnamurti and Bhalme, 1976; Chen and Murakami, 1988; Annamalai and Slingo, 2001), more complex mean flow that the ISO interacts with (e.g., Teng and Wang, 2003; Yang et al., 2008), as well as the greater heterogeneity of the underlying surface conditions and topography that the ISO is influenced by (e.g., Liu et al., 2007). The performances of the Asian monsoon boreal summer ISO in numerical settings not only share some similar shortcomings with the MJO simulations but also have their unique problems. For instance, the study by Waliser et al. (2003) examined ten atmospheric general circulation model (AGCM) simulations to assess their representations of low frequency ISO variability associated with the Asian summer monsoon. Their results show that the ISO patterns in seven of the ten AGCMs lack sufficient eastward propagation, have smaller zonal and meridional spatial scales than the observed patterns, and often have a southwest-northeast tilt of the rain belt rather than the observed northwest-southeast tilt over the Indian Ocean.

Most previous studies of boreal summer ISO modeling are focused on the lower frequency band (namely the MJO time scale) and their concerned regions are over the western tropical North Pacific (WNP) and the Indian monsoon region. Based on observations, ISOs with various periodicities potentially affect the East Asia (EA)-WNP summer monsoon variation (e.g., Chen and Chen, 1995; Zhang et al., 2002; Chan et al., 2002; Yang and Li, 2003). Thereby, it is necessary to provide a comprehensive evaluation of the ISO simulation over the EA-WNP summer monsoon region. In particular, the subtropical EA monsoon ISO has unique characteristics of midlatitude variation (e.g., Zhang et al., 2003; Mao and Wu, 2006; Yang et al., 2008). However, in previous model evaluations, the higher frequency ISOs (e.g., the quasi-biweekly) and the ISO over the subtropical EA region have been less concerned.

Climatological ISO (CISO) and transient ISO (TISO), as two objective measures, are applied to validate the simulation of the EA-WNP summer ISO (Yang et al., 2008). The CISO represents the phase-locked component of ISO (Wang and Xu, 1997). Compared to the slow annual cycle, it is a part of the "fast" annual cycle (LinHo and Wang, 2002), which describes seasonal march (e.g., Ding, 1992; Nakazawa, 1992; Tanaka, 1992; Ueda et al., 1995) and the multi-stage onset of the Asian summer monsoon (Lau et al., 1988; Wu and Wang, 2001; Wang and LinHo, 2002). The TISO is defined as the remaining part after removing CISO from the total ISO, which represents the year-to-year varying portion of ISO. These two portions of ISO have been found to have different features and different contributions to the total ISO. For instance, during the summer of 1998 that includes two intraseasonal rainfall events, the first flooding event is mainly associated with CISO and the second is contributed by TISO (Yang et al., 2008). Therefore, this approach, which distinguishes CISO and TISO, is advantageous and necessary in evaluating the summer ISO over the EA-WNP sector.

This paper will be organized as follows. Firstly, the observational data, model and methodology are described in section 2. In section 3, we focus on the evaluations of the basic performances of the simulated CISO and TISO in an atmospheric general circulation model with a comparison to the observations. In section 4, we attempt to find possible factors responsible for model discrepancies in simulating the ISO over the EA-WNP. Finally the conclusion and discussion are given in section 5.

2. Observational data, model and methodology

2.1 *Observational data*

The datasets applied to document the observed ISO in convective activity and precipitation are retrieved from the following three sources: (1) National Oceanic and Atmospheric Administration (NOAA) interpolated daily outgoing longwave radiation (OLR) (Liebmann and Smith, 1996) from 1979 to 2005, which is basically regarded as a reasonable substitute of rainfall and high clouds, especially in the tropical regions; (2) the monthly precipitation data from 1979 to 2005, which are retrieved from the Global Precipitation Climatology Project (GPCP) (Huffmann et al., 1997); and (3) a newly-released high-quality East Asian daily precipitation data on land (EA-Pre/L hereafter) from NOAA/Climate prediction Center (CPC) (Xie et al., 2007), which has been constructed based on 2200 stations' observations over East Asia (5°–60°N, 65°–155°E) from 1979 to 2005.

To obtain the climatological mean states of circulation, we use the datasets from the National Center for Environmental Prediction-Department of Energy (NCEP-DOE) Reanalysis 2 (NCEP2) between 1979 and 2005 (Kanamitsu et al., 2002).

2.2 *Model description*

GAMIL 1.1.1 is the latest version of a grid-point atmospheric general circulation model (GAMIL), which

is developed at the State Key Laboratory for Numerical Modeling of Atmospheric Science and Geophysical Fluid Dynamics (LASG) in Institute of Atmospheric Physics (IAP) of Chinese Academy of Sciences (Wang et al., 2004). Its dynamical core is based on a finite difference scheme that satisfies the conservation law of total mass and the effective energy for solving the primitive hydrostatic equations of baroclinic atmosphere. Except for two optional mass flux convection schemes: the Tiedtke scheme (Tiedtke, 1989; Nordeng, 1994; Liu et al., 2005) and the Zhang-McFarlan scheme (Zhang and McFarlane, 1995), its physical packages are completely the same as those in the National Center for Atmospheric Research (NACR) community atmospheric Model Version 2 (CAM2) (Collines et al., 2003). The cumulus parameterization scheme used for the current study is the Tiedtke scheme. This new version that we evaluate in the study additionally includes the modifications made to both the Tiedtke convective scheme (Li, 2007) and the parameterization of cloud properties (Li, 2007). The spatial resolutions are $2.8^\circ \times 2.8^\circ$ in the horizontal and 26 levels in the vertical.

We made a 31-year AMIP (Atmospheric Model Intercomparison Project) (Phillips, 1996) run from 1975 to 2005, constrained by realistic sea surface temperature and sea ice. In order to remove the effect of the spin-up process as well as match the historical record in observations, we used the latter 27-year daily output from 1979 to 2005 for the assessment of ISO.

2.3 *Statistic methodology*

In order to extract the CISO component, we began by removing the first three Fourier harmonics (slow annual cycle portion) from the climatological daily mean time series and made a 5-day running mean to remove the synoptic signals. Then, both the slow annual cycle and the CISO components were subtracted from the raw daily time series of a particular year. Finally, time-filtering, based on the Fourier harmonic analysis, was applied to obtain the time series of the TISO.

Since the filtered data involve high autocorrelations between consecutive daily values, the degree of freedom is much less than the original sample size. Using Chen's (1982) method, the effective degree of freedom was calculated for each variable at each grid. Based on the effective degree of freedom, a t-test was applied for the significance test of a point-based lead-lag correlation analysis. The t-test was also used to examine the significance level of CISO based on the null hypothesis that the observed sample mean (the amplitude of CISO) at a fixed date was drawn from a population characterized by a zero mean, namely that the amplitude of CISO at a fixed date is not significantly different from zero (Wang and Xu, 1997).

The Fast Fourier Transform method (FFT) with a tapered window, which is one of the most common methods of spectral analysis, is applied to select the dominant periodicities of TISO in a particular year. In order to measure the significance of a multi-year mean spectrum, the corresponding red noise spectrum is obtained by averaging multi-year theoretical Markov "red noise" spectrums of background. The 95% confidence bound is calculated against this mean red noise spectrum.

3. EA-WNP boreal summer ISO in GAMIL 1.1.1

3.1 *Simulation of CISO in GAMIL 1.1.1*

The northward advance of the EA rain belt has been widely recognized (e.g., Yeh et al., 1958; Zhu and Song, 1979; Tao and Chen, 1987; Ding, 2004). This seasonal march is best depicted by the CISO (Yang et al., 2008; Liu et al., 2008). Therefore, the validation of CISO focuses on its meridional propagation over the EA-WNP longitudes.

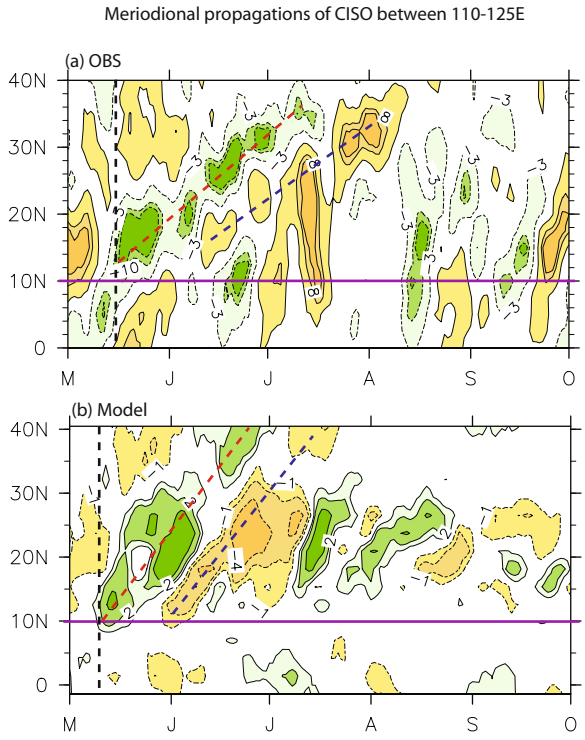

Fig. 1. Meridional propagations of CISO along the longitudes between 110°E and 125°E: detected from (a) observed daily OLR and (b) GAMIL 1.1.1 daily precipitation. Yellow shading represents a dry anomaly and green shading represents a wet anomaly (the same hereafter). The shaded portion of CISO is statistically significant above the 95% confidence level. Units: W m^{-2} for OLR and mm d^{-1} for precipitation.

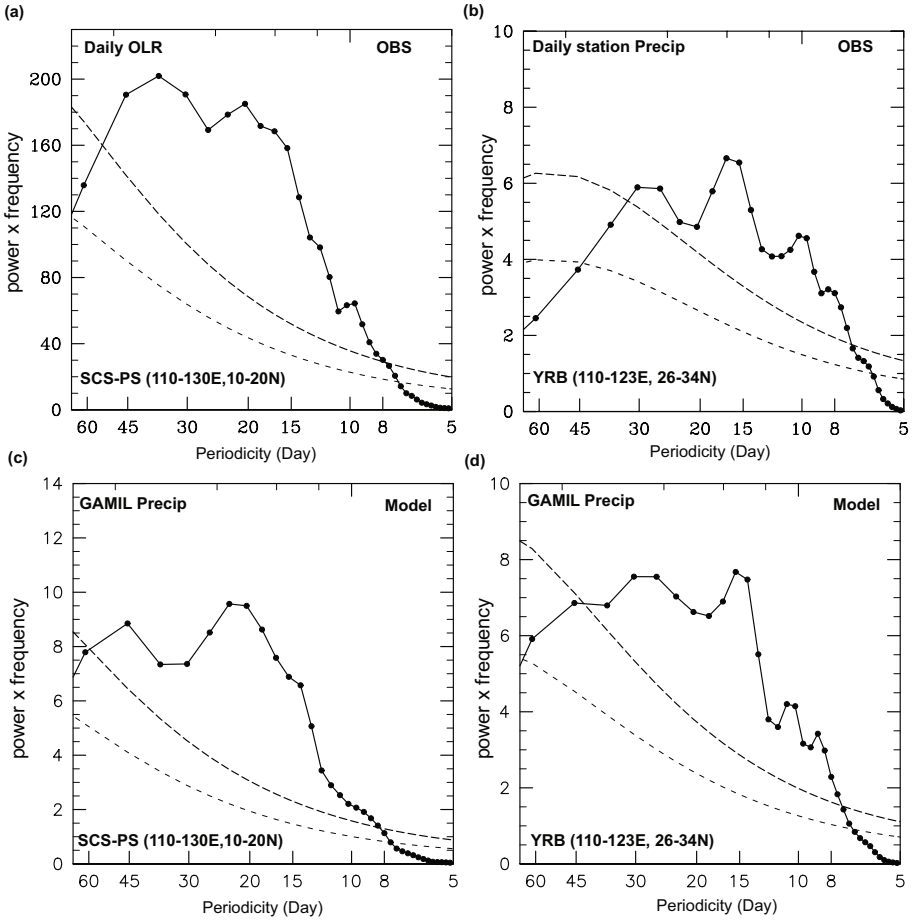

Fig. 2. Mean power spectrums of TISO calculated for 27 summers during 1979–2005, over the SCS-PS (the left column) and the YRB (the right column). Panels (a) and (b) are calculated from observations; Panels (c) and (d) are from simulations. The thin dashed line denotes the Markov red noise spectrum and the thick dashed line indicates the 95% confidence bound. x abscissa has been rescaled into the natural logarithm of the frequency.

Figure 1 exhibits the meridional march of CISO between 110°E and 125°E during the boreal summer in observation and simulation. Compared with the observed, GAMIL1.1.1 can successfully reproduce the following features: (1) the stepwise northward propagation of the rainfall from 15°N to 40°N; (2) two northward propagating dry spells respectively occurring prior to and after the rainfall season; (3) and the CISO signal becomes much weaker after mid-August.

The most noteworthy discrepancy between the observation and simulation are manifested in the timing of the wet/dry CISO phase occurrences. Two major problems are (a) the onset of the first wet phase over SCS latitudes, which signals the climatological onset of the SCS summer monsoon, is around 6–7 days earlier than observation, and (b) the northward migration of the rain belt as depicted by the first wet phase, is too fast with a speed of 0.58 latitude degrees per day while the observed speed is 0.42 latitude degrees per day. Accordingly, the dry phase of CISO, which occurs after the wet phase ends, also comes early in the simulation. In addition, the CISO signals in the model are rather weak over the tropical regions to the south of 10°N.

3.2 *Simulation of TISO in GAMIL 1.1.1*

In this section, the basic performances of the simulated TISO are evaluated from two typical aspects, the dominant periodicities and associated propagations, respectively over the South China Sea-Philippine Sea (SCS-PS: 10°–20°N, 110°–130°E) and the Yangtze River Basin (YRB: 26°–34°N, 110°–123°E). Extensive sensitivity experiments have been done with different domains of the tropical WNP and the subtropical EA, and it was found that the dominant periodicities and characteristics of TISOs over the above two domains

can capture the major features of TISO, respectively, in the tropics and the subtropics over the EA-WNP region.

3.2.1 *Simulation of dominant periodicities*

In observation, the dominant periodicities of TISO over the two regions (SCS-PS and YRB) are identified through multi-year mean spectrums of 27 summers (May to October) during 1979–2005, as shown in Figs. 2a and 2b. Considering the reliability of observational datasets, OLR is used over the SCS-PS and the EA-Pre/L data is applied over the YRB region. As a result, 30–50-day, 12–25-day and 8–11-day are three major TISO frequency bands over the SCS-PS region (Fig. 2a); and quasi-30-day (23–36-day), quasi-16-day (13–20-day) and quasi-10-day (9–12-day) are three dominant TISO modes of summer precipitation over the YRB region (Fig. 2b).

Compared with observation, the two major TISO modes over the SCS-PS region, namely 12–25-day and 30–50-day, can be captured in the spectral analysis from the model (Fig. 2c). The variance of the simulated lower frequency (30–50-day) peak, however, is relatively underestimated compared to the 12–25-day mode. The 8–11-day peak in the SCS-PS summer precipitation almost disappears in the simulation. Over the YRB, the three dominant TISO modes during the boreal summer can be well distinguishable in the model (Fig. 2d).

In observation, the 12–25-day and 30–50-day TISO modes account for 33% and 34%, respectively, to the total ISO over the SCS-PS, whereas the contribution from the 8–11-day is only 8%. On the other hand, the quasi-30-day, quasi-16-day, and quasi-10-day contributes 22%, 21%, and 12%, respectively, to the total ISO in the YRB summer precipitation. Therefore, our following evaluations on the propagating features are primarily made for the two major TISO modes over

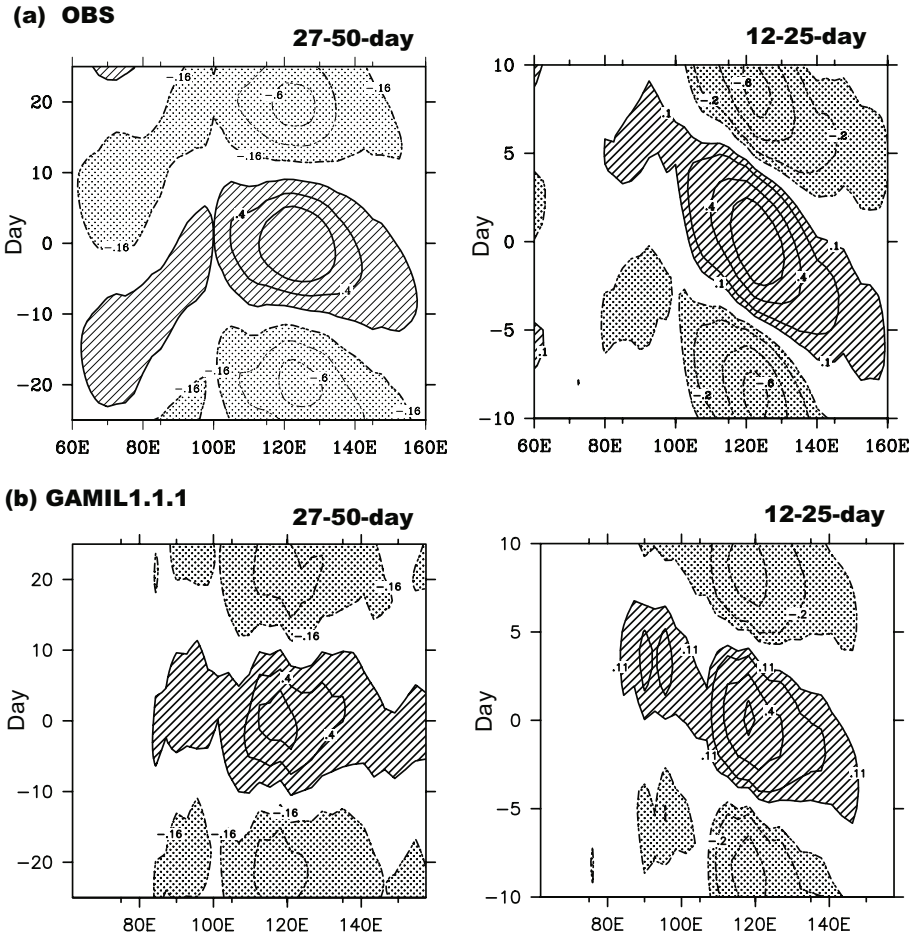

Fig. 3. Zonal propagations of 30–50 day (the left column) and 12–25-day (the right column) TISO modes averaged along the latitudes between 10°N and 20°N, respectively, based on (a) observed OLR (upper panels) and (b) model precipitation (lower panels), calculated by point-based lead-lag correlation analysis with reference to the SCS-PS region. Gridded are the regions above the 0.05 significance test.

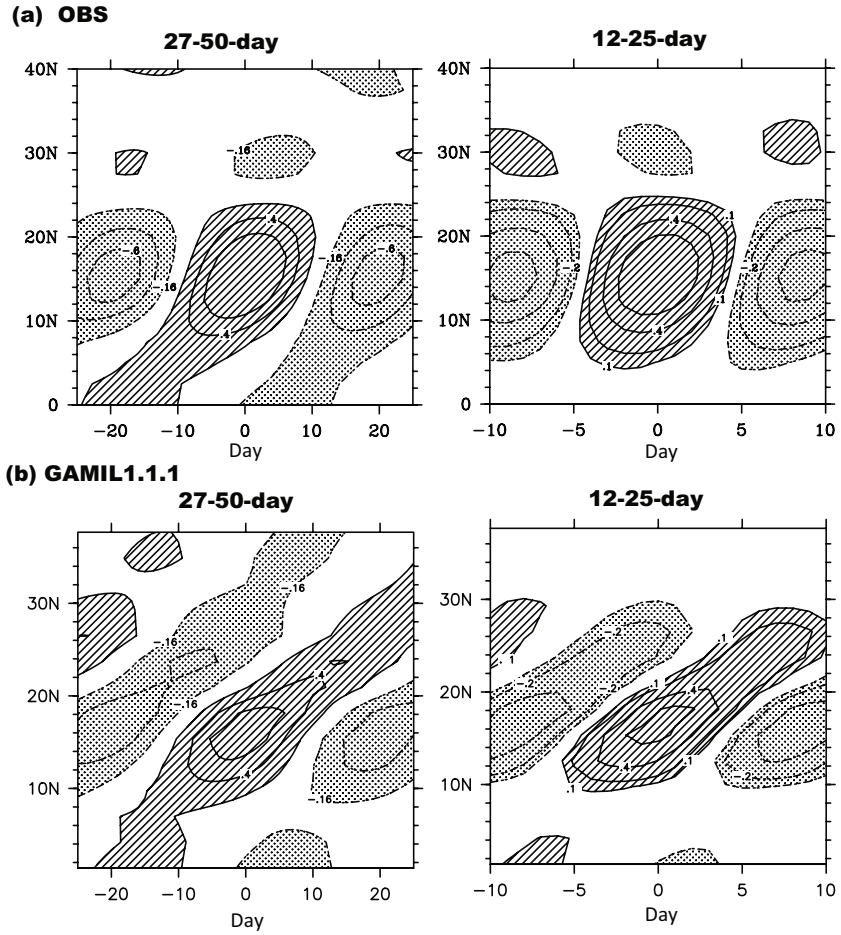

Fig. 4. Meridional propagations of 30–50-day (the left column) and 12–25-day (the right column) TISO modes averaged along the longitudes between 110°E and 120°E, respectively, based on (a) observed OLR (upper panels) and (b) model precipitation (lower panels), calculated by point-based lead-lag correlation analysis with reference to the SCS-PS region. Gridded are the regions above the 0.05 significance test.

the SCS (12–25-day and 30–50-day) and three TISO modes over the YRB (quasi-30-day, quasi-16-day, and quasi-10-day). These TISO modes are considered to be the most important for the EA-WNP summer monsoon intraseasonal prediction.

3.2.2 *Simulation of propagation of major TISO modes*

We evaluate the propagations of the major TISO modes through a series of Hovmoller diagrams (Figs. 3, 4, 5, and 6) of precipitation or convection. These Hovmoller diagrams are obtained through the point-based lead-lag correlation analysis with reference to the convection over the SCS-PS and precipitation over the YRB for each TISO component respectively. For the TISO modes over the SCS-PS region, their zonal propagations are along the latitudes between 10°–20°N (Fig. 3) and their meridional propagations are shown along the longitudes between 110°E and 120°E (Fig. 4). Over the YRB, the zonal and meridional propagations of the associated TISO modes are shown between 26°N and 34°N (Fig. 5) and between 110°E and 123°E (Fig. 6), respectively.

In observation, the 30–50-day mode is primarily characterized by an eastward propagation over the Indian Ocean longitudes (Fig. 3a) and northward propagation over the SCS longitudes (Fig. 4a), while the 12–25-day mode mainly exhibits a westward propagation from the western Pacific (around 160°E) along the SCS latitudes (Fig. 3a). The propagations of the two major TISO modes over the SCS-PS depicted here are consistent with many previous studies (Chen and Murakami, 1988; Wang and Rui, 1990; Lawrence and Webster, 2002; Hsu et al., 2004). In the model (Fig. 3b and Fig. 4b), we notice that the northward propagation of the 30–50-day and the westward propagation

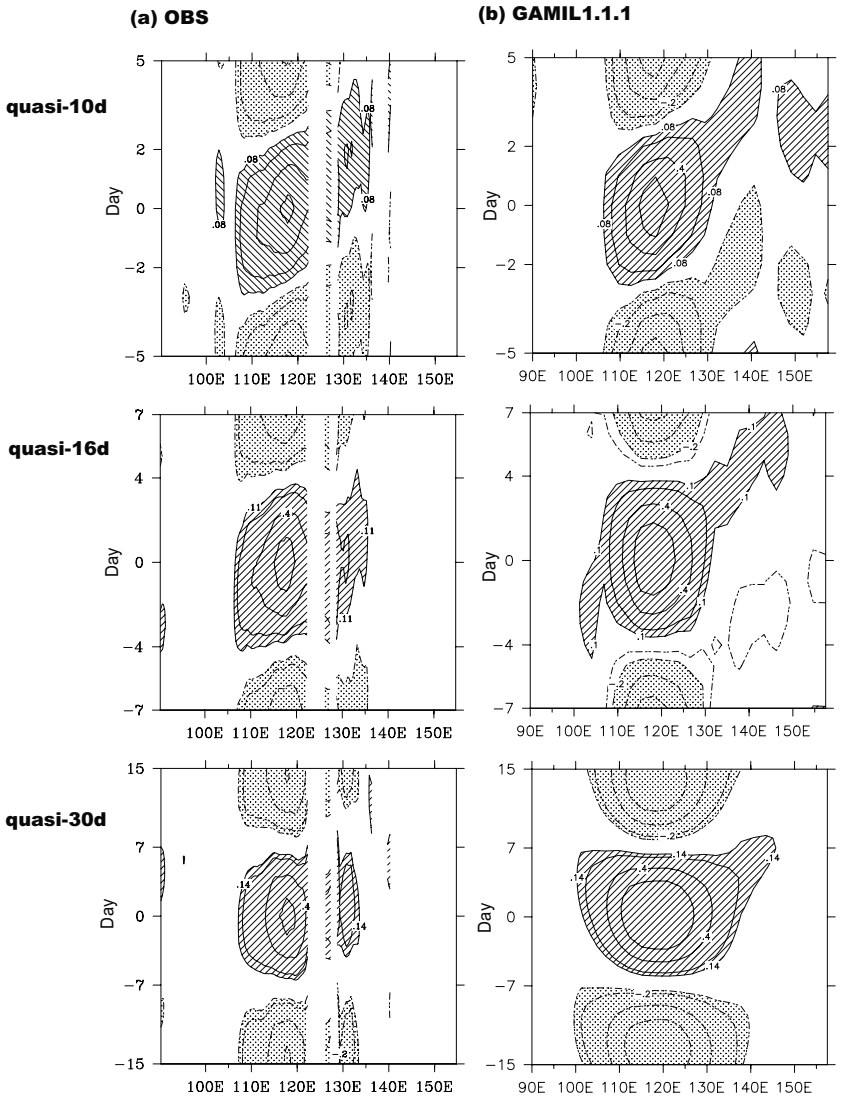

Fig. 5. Zonal propagations of three TISO modes averaged along the latitudes between 26°N and 34°N, respectively, based on (a) observed precipitation (left column) and (b) model precipitation (right column), calculated by point-based lead-lag correlation analysis with reference to the YRB region. Gridded are the regions above the 0.05 significance test.

of the 12–25-day are well simulated over the SCS-PS region. However, the model fails to simulate the eastward propagation of the 30–50-day to the west of 100°E. Moreover, the model produces an excessively northward propagation north of 20°N in the two TISO modes over the SCS-PS region.

In the subtropics (or the YRB), both quasi-10-day and quasi-16-day modes are characterized with a southeastward propagation over the YRB in observation, whereas the quasi-30-day mode appears quasi-stationary (Fig. 5a and Fig. 6a). Compared with the observed, the zonal propagations of the three modes are well simulated (Fig. 5b), however, the model fails to reproduce the realistic meridional propagations. In particular, both the simulated quasi-10-day and quasi-16-day modes exhibit a northward propagation rather than a southward propagation in the observations (Fig. 6b).

4. What contributes to the deficiencies in the ISO simulation?

4.1 *Possible explanations of the deficiencies in the simulated CISO*

One of the noticeable deficiencies in the CISO simulation is the earlier onset of the SCS summer monsoon, i.e., the first significant wet phase of CISO during the boreal summer. Since SST is realistic in the AMIP

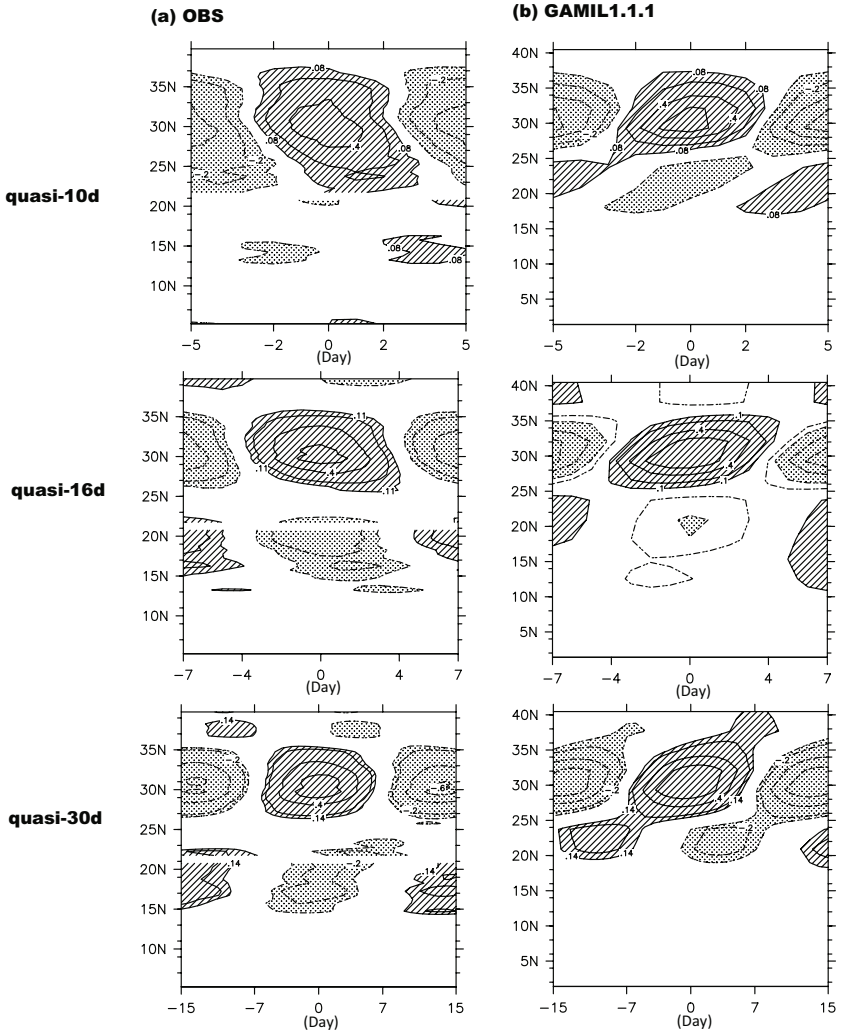

Fig. 6. Meridional propagations of three TISO modes averaged along the longitudes between 110°E and 123°E, respectively, based on (a) observed precipitation (left column) and (b) model precipitation (right column), calculated by point-based lead-lag correlation analysis with reference to the YRB region. Gridded are the regions above the 0.05 significance test.

simulation, there is no deficiency in the SST seasonal migration. Many previous studies have found that the land-sea thermal contrast during the pre-monsoon season is very important for the SCS summer monsoon onset (He et al., 1987; Yanai et al., 1992; Ose, 1998). Thereby, the deficiency in the simulated land-sea thermal contrast is assumed to be one of the possible reasons for the early onset. Figure 7a shows that the simulation yields warmer than observed surface temperatures over the Eurasian continent during April–May, especially over India, the Indonesia Peninsular, and the Tibet Plateau, which may result in an increased land-sea thermal contrast over the Asian monsoon region. The enhanced land-sea thermal contrast may induce excessive lower level westerly wind along the southern flank of the Asian continent (Fig. 7b) and thereby trigger the early onset of the SCS summer monsoon rainfall.

Another weakness in the model simulation is the fast northward march of rainfall (the first wet phase of CISO) during the early boreal summer. Wu and Wang (2001) have proposed that the northward multi-stage march of the summer monsoon is evidently associated with the behaviors of the WNP subtropical high and the monsoon trough. Therefore, the fast northward march of CISO in the model could be ascribed to the erroneous eastward retreat of the WNP subtropical high and northward shift of the monsoon trough in the simulation as illustrated in Fig. 8.

Furthermore, in the model, the northward shift of the seasonal mean western Pacific monsoon trough rainfall from 5°N to 20°N may account for the absence

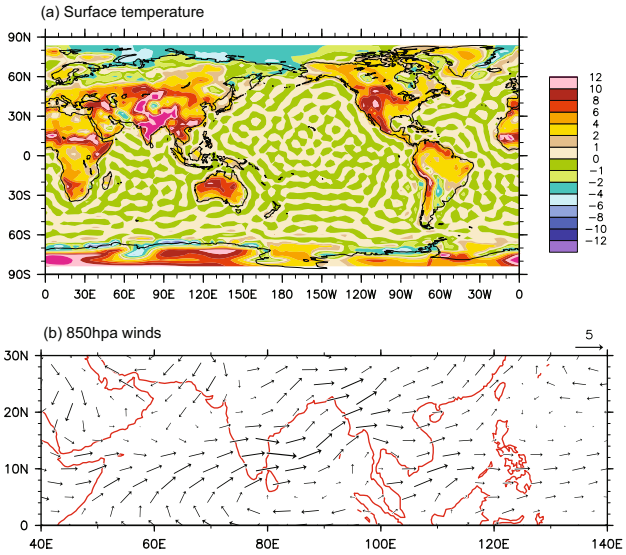

Fig. 7. Difference of climatological early summer (April–May) (a) surface temperature (units: K), and (b) 850 hPa winds (units: m s^{-1}) between GAMIL 1.1.1 and observation.

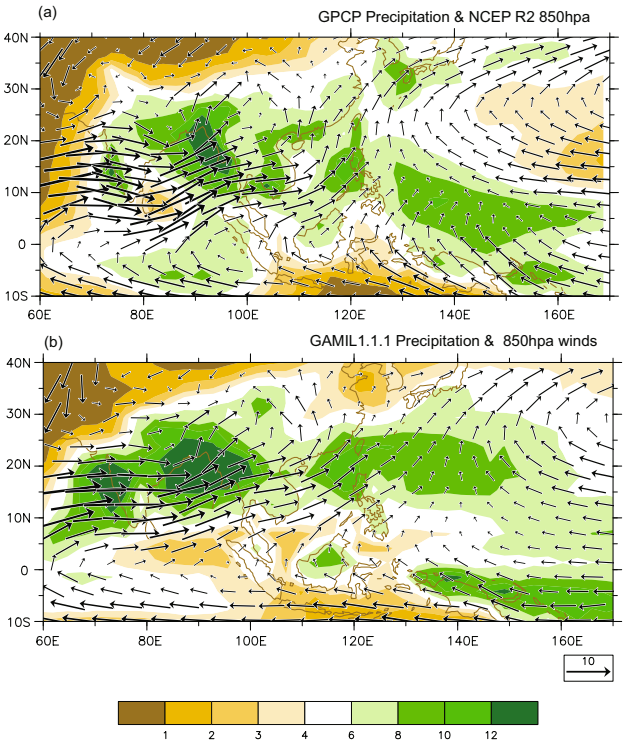

Fig. 8. Climatological summer (Jun–Jul–Aug) 850 hPa winds (vectors) and precipitations (shadings) in (a) observation and (b) GAMIL 1.1.1, units: m s^{-1} for winds and mm d^{-1} for precipitation.

of the simulated CISO signal south of 10°N.

4.2 *Possible explanations of the deficiencies in the simulated TISO*

Over the SCS latitudes, the most distinguishable model deficiency in simulating the 30–50-day TISO mode is the rather weak eastward propagation to the west of 100°E. This weakness could be largely associated with the poor representation of the eastward propagating MJO signal along the equator in the model (Fig. 9). The drier conditions over the equatorial central-eastern Indian Ocean in the simulated basic state (Fig. 8) could be one of the factors which cause the weak eastward propagation, because the equatorial central-eastern IO is the source region where the SCS 30–50-day mode stems from and develops (Yang et al., 2008). Noteworthy is that both the periodicity and the northward propagation of this lower frequency TISO mode are still reasonably captured in simulation without the presence of the eastward propagating component. This phenomenon indicates that the 30–50-day mode over the SCS-PS region includes two types of northward propagation: one is connected with the eastward propagating MJO and the other is independent of the eastward propagating MJO. The "independent northward propagation" has been found by several previous observational findings (e.g., Wang and Rui, 1990; Jiang et al., 2004). This model only captures the "independent northward" component of the 30–50-day mode but loses the eastward propagation-related northward propagation, which could partly account for the reduced variance of this TISO mode in the spectral analysis in the model (Fig. 2c).

In the subtropics, the model fails to capture the southward propagation of the quasi-10-day and quasi-16-day mode over the YRB longitudes. According to the study from Yang et al. (2008), the occurrence of the quasi-10-day and quasi-16-day modes over the YRB is closely linked to the southward propagation of the upper-level perturbations from higher latitudes. In model climatology, the maximum center of the 200 hPa westerly jet is weaker than observed and is displaced westward compared to the observed (Fig. 11), and the deceleration region of the upper-level jet shifts westward accordingly. Consequently, the high-latitude upper-level transient perturbation might emanate equatorward to the west of the subtropical EA longitudes in the model, thus the realistic southward propagation over the subtropical EA longitudes disappears.

5. Conclusion and discussion

In this study, the basic performances of the boreal summer ISO have been evaluated for GAMIL1.1.1's

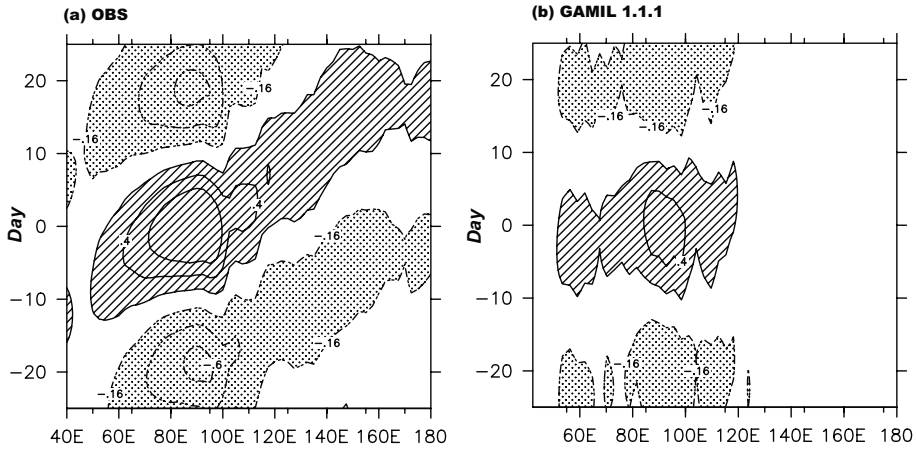

Fig. 9. Zonal propagations of 30–50-day TISO mode along the equator between 5°N and 5°S during boreal summer, calculated by point-based correlation analysis with reference to the eastern equatorial Indian Ocean (5°–5°N, 85°–95°E), revealed by (a) observed daily OLR and (b) GAMIL 1.1.1 daily precipitation. The y-axis is united with "day".

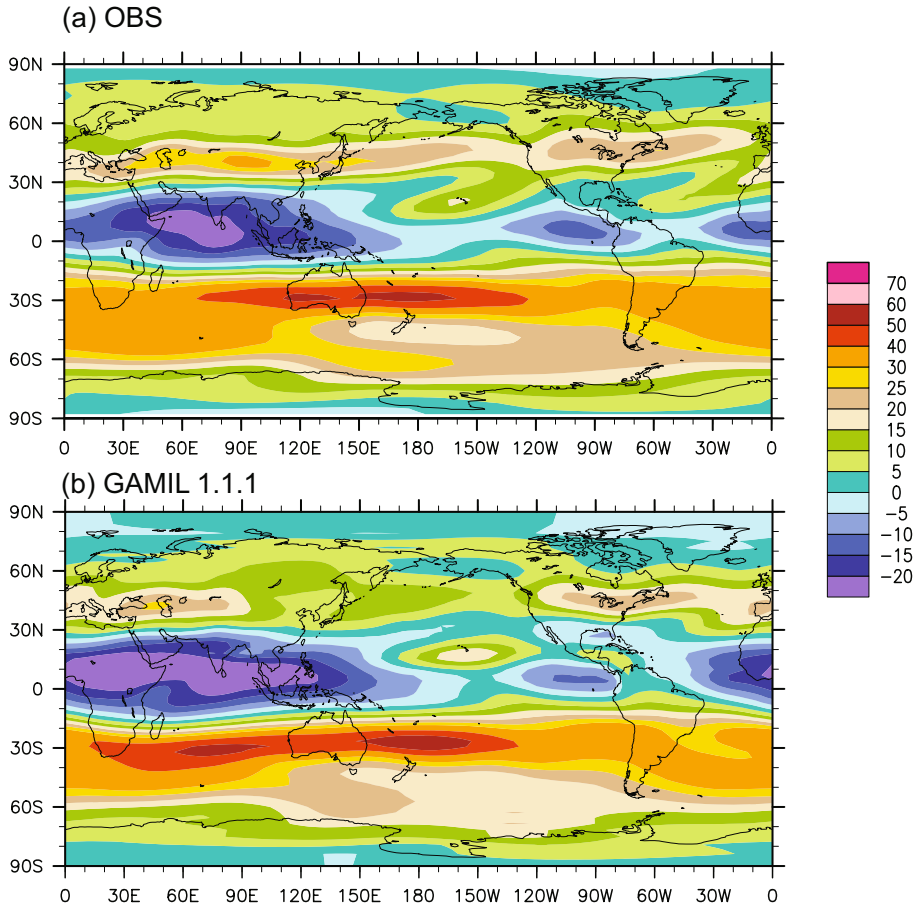

Fig. 10. Climatological summer (Jun–Jul–Aug) 200 hPa zonal winds in (a) observation (NCEP R2) and (b) GAMIL 1.1.1, units: m s^{-1}.

27-year AMIP simulation through two measures: CISO and TISO. The CISO represents the portion of ISO that is phase locked to the annual cycle, while the TISO is the year-to-year varying portion of ISO. A series of validations indicate that many observed features of CISO and TISO can be reasonably captured in this model, primarily including the stepwise northward march of the rain belt of CISO, the major TISO periodicities in both the tropical WNP and the subtropical EA regions, the northward propagation of the 30–50-day and the westward propagation of 12–25-day TISO modes over the SCS-PS, and the zonal propagations of the YRB TISO modes.

However, the simulation has noteworthy weaknesses. The deficiencies in the simulated CISO mainly include the earlier onset of the SCS monsoon, the quickened northward propagation from 20°N to 40°N, and the absence of the CISO signal to the south of 10°N. The TISO simulation fails to capture the observed eastward propagation of the 30–50-day TISO mode and the southward propagations of the YRB TISO modes. Additionally, most TISO modes in the model falsely exhibit the overwhelming northward propagations to the north of 20°N.

We find that many deficiencies in the simulation of CISO and TISO are associated with the model's biases in mean states. These mean state biases primarily include the drier conditions over the equatorial central-eastern Indian Ocean, the northward shift of the western Pacific monsoon trough, the eastward retreat of the WNP subtropical high, and the westward shift of the subtropical westerly jet, which may cause erroneous genesis or the development of intraseasonal perturbations. In addition, the land surface thermal condition is suggested to be another influential factor for the ISO simulation through modifying the land-sea thermal contrast. The close linkage between the ISO simulation and the mean state simulation provide guidance for the model development.

As a by-product of model evaluation, we also find the northward propagation of the 30–50-day mode includes two components: one is linked to the eastward propagation of the MJO and the other is independent of the eastward propagating MJO. The finding of the "independent northward propagation" supports several previous observational studies.

Lacking a generally accepted mechanism on the genesis of the subtropical EA summer ISO potentially counteracts our understanding of the deficiencies in the subtropical EA summer ISO simulations. Therefore, more studies from observations and theoretical models of the subtropical EA ISO need to be encouraged in the future.

Furthermore, the validation of the boreal summer ISO simulation over the EA-WNP region is suggested to be made in broader fields, including multi-model evaluation to find the common advantages and disadvantages of the ISO simulation and the assessment of air-sea coupling models to investigate the effects of air-sea coupling (Kemball-Cook et al., 2000; Fu et al., 2003; Fu and Wang, 2004) on the EA-WNP ISO simulation. The impacts of land processes on the EA-WNP summer ISO simulation and prediction also calls for in-depth studies.

Acknowledgements. The work is supported by the Innovative Research Group Funds (Grant No. 408210921), the CAS International Partnership Project, the 973 Project (Grant Nos. 2005CB321703 and 2006CB403602), and fund from State Key Laboratory of Earth Surface Processes and Resource Ecology (No. 070205) in Beijing Normal University. The model integration is performed on the Lenovo Deep Comp 6800 Supercomputer at the supercomputing Center of the Chinese Academy of Sciences.

REFERENCES

Annamalai, H., and J. M. Slingo, 2001: Active/break cycles: Diagnosis of the intraseasonal variability of the Asian Summer Monsoon. *Climate. Dyn.*, **18**, 85–102.

Chao, W. C., and L. Deng, 1998: Tropical intraseasonal oscillation, super cloud clusters, and cumulus convection schemes. Part II: 3D aquaplanet simulations. *J. Atmos. Sci.*, **55**, 690–709.

Chan, J. C. L., W. Ai, and J. Xu, 2002: Mechanisms responsible for the maintenance of the 1998 South China Sea summer monsoon. *J. Meteor. Soc. Japan.*, **80**, 1103–1113.

Chen, T. C., and J. R. Chen, 1995: An observational study of the South China Sea Monsoon during the 1979 summer—Onset and life-cycle. *Mon. Wea. Rev.*, **123**, 2295–2318.

Chen, T. C., and M. Murakami, 1988: The 30–50 day variation of convective activity over the Western Pacific-Ocean with emphasis on the northwestern region. *Mon. Wea. Rev.*, **116**, 892–906.

Chen, W. Y., 1982: Fluctuations in Northern Hemisphere 700 mb height field associated with southern oscillation. *Mon. Wea. Rev.*, **110**, 808–83.

Collins, W. D., and Coauthors, 2003: Description of the NCAR Community Atmosphere Model (CAM2). National Center For Atmospheric Research, Boulder, 171pp.

Ding, Y. H., 1992: Summer monsoon rainfall in China. *J. Meteor. Soc. Japan*, **70**, 373–396.

Ding, Y. H., 2004: Seasonal march of the East Asian summer monsoon in the East Asian Monsoon. *The East Asian Monsoon*, C. P. Chang, Ed., World Scientific Publisher, Singapore, 564pp.

Fu, X., and B. Wang, 2004: Different solutions of intraseasonal oscillation exist in atmosphere ocean coupled model and atmosphere-only model. *J. Climate*, **17**,

1263–1271.

Fu, X., B. Wang, T. Li, and J. P. McCreary, 2003: Coupling between northward propa- gating intraseasonal oscillations and sea-surface temperature in the Indian Ocean. *J. Atmos. Sci.*, **60**, 1733–1753.

He, H. Y., J. W. McGinnis, Z. S. Song, and M. Yanai, 1987: Onset of the Asian summer monsoon in 1979 and the effects of the Tibetan Plateau. *Mon. Wea. Rev.*, **115**, 1966–1995.

Hsu, H. H., C.-H. Weng, and C.-H. Wu, 2004: Contrasting characteristics between the northward and eastward propagation of the intraseasonal oscillation during the boreal summer. *J. Climate*, **17**, 727–743.

Huffmann, G. J., and Coauthors, 1997: The global precipitation climatology project (GPCP) combined precipitation dataset. *Bull. Amer. Meteor. Soc.*, **78**, 5–20.

Jiang, X., T. Li, and B. Wang, 2004: Structures and mechanisms of the northward propagating boreal summer intraseasonal oscillation. *J. Climate*, **17**, 1022–1039.

Kanamitsu, M., W. Ebisuzaki, J. Woollen, S. K. Yang, J. J. Hnilo, M. Fiorino, and G. L. Potter, 2002: NCEP-Doe AMPI-II Reanalysis (R-2). *Bull. Amer. Meteor. Soc.*, **83**, 1631–1643.

Kemball-Cook, S., B. Wang, and X. Fu, 2000: Simulation of the ISO in the ECHAM4 model: The impact of coupling with an ocean model. *J. Atmos. Sci.*, **59**, 1433–1453.

Krishnamurti, T. N., and H. N. Bhalme, 1976: Oscillations of a monsoon system. Part 1: Observational aspects. *J. Atmos. Sci.*, **33**, 1937–1954.

Lau, K. M., G. J. Yang, and S. H. Shen, 1988: Seasonal and intraseasonal climatology of summer monsoon rainfall over East Asia. *Mon. Wea. Rev.*, **116**, 18–37.

Lawrence, D. M, and P. J. Webster, 2002: The boreal summer intraseasonal oscillation: Relationship between northward and eastward movement of convection. *J. Atmos. Sci.*, **59**, 1593–1606.

Lee, M. I., I. S. Kang, B. E. Maps, and P. J. Webster, 2003: Impacts of cumulus convection parameterization on aqua-planet AGCM simulations of tropical intraseasonal variability. *J. Meteor. Soc. Japan.*, **81**, 963–992.

Li, L. J., B. Wang, Y. Q. Wang, and H. Wan, 2007: Improvements in climate simulation with modifications to the Tiedtke convective parameterization in the Grid-Point Atmospheric Model of IAP LASG (GAMIL). *Adv. Atmos. Sci.*, **24**, 323-335, doi: 10.1007/s00376-007-0323-3.

Li, L. J., 2007: Improvements and simulations of convective and cloud-radiation parameterizations in GAMIL. Ph.D. dissertation, Insititute of Atmospheric Physics, Chinese Academy of Sciences, 107pp. (in Chineses)

Liebmann, B., and C. A. Smith, 1996: Description of a complete (interpolated) outgoing longwave radiation dataset. *Bull. Amer. Meteor. Soc.*, **77**, 1275–1277.

Lin, J. L., and Coauthors, 2006: Tropical intraseasonal variability in 14 IPCC AR4 climate models. Part I: Convective signals. *J. Climate*, **19**, 2665–2690.

LinHo, and B. Wang, 2002: The time-space structure of the Asian-Pacific summer monsoon: A fast annual cycle view. *J. Climate*, **15**, 2001–2019.

Liu, P., B. Wang, K. Sperber, and J. Meehl, 2005: MJO in the NCAR CAM2 with the Tiedtke convection scheme. *J. Climate*, **18**, 3007–3020.

Liu, J., B. Wang, and J. Yang, 2008: Forced and internal modes of variability of the East Asian summer monsoon. *Climate of the Past Discussion*, Special Issue: S15, **4**, 1–9.

Liu, Y. M., Q. Bao, A. M. Duan, Z. A. Qian, and G. X. Wu, 2007: Recent progress in the impact of the Tibetan Plateau on Climate in China. *Adv. Atmos. Sci.*, **24**, 1060–1076, doi: 10.1007/s00376-007-1060-3.

Madden, R. A, and P. R. Julian, 1971: Detection of a 40–50 day oscillation in the zonal wind in the tropical Pacific. *J. Atmos. Sci.*, **28**, 702–708.

Mao, J. Y., and G. X. Wu, 2006: Intraseasonal variations of the Yangtze rainfall and its related atmospheric circulation features during the 1991 summer. *Climate Dyn.*, **27**, 815–830.

Nakazawa, T., 1992: Seasonal phase lock of intraseasonal variation during the Asian Summer Monsoon. *J. Meteor. Soc. Japan*, **70**, 597–611.

Nordeng, T. E., 1994: Extended versions of the convective parameterization scheme at ECMWF and their impact on the mean and transient activity of the model in the Tropics. *ECMWF Research Department Tech. Memo.*, No. 206, 41pp.

Ose, T., 1998: Seasonal change of Asian summer monsoon circulation and its heat source. *J. Meteor. Soc. Japan*, **76**, 1045–1063.

Phillips, T. J., 1996: Documentation of the AMIP models on the World Wide Web. *Bull. Amer. Meteor. Soc.*, **6**, 1191–1196.

Slingo, J. M., and R. A. Madden, 1991: Characteristics of the tropical intraseasonal oscillation in the NCAR community climate model. *Quart. J. Roy. Meteor. Soc.*, **117**, 1129–1169.

Slingo, J. M., and Coauthors, 1996: Intraseasonal oscillations in 15 atmospheric general circulation models: Results from an AMIP diagnostic subproject. *Climate Dyn.*, **12**, 325–357.

Sperber, K. R., 2004: Madden-Julian variability in NCAR CAM2.0 and CCSM2.0. *Climate Dyn.*, **23**, 259–278.

Tanaka, M., 1992: Intraseasonal oscillation and onset and retreat dates of the summer monsoon over east, Southeast Asia and the western Pacific region using GMS high cloud amount data. *J. Meteor. Soc. Japan*, **70**, 613–629.

Tao, S., and L. X. Chen, 1987: A review of recent research on the East Asian summer monsoon in China. Monsoon Meteorology, C.-P. Chang and T. N. Krishnamurti, Eds., Oxford University Press, 60–92.

Teng, H. Y., and B. Wang, 2003: Interannual variations of the boreal summer intraseasonal oscillation in the Asian-Pacific region. *J. Climate*, **16**, 3572–3584.

Tiedtke, M., 1989: A comprehensive mass flux scheme for cumulus parameterization in large-scale models. *Mon. Wea. Rev.*, **117**, 779–1800.

Ueda, G., T. Yasunari, and R. Kawamura, 1995: Abrupt seasonal changes of large-scale convective activity over the western Pacific in the northern summer. *J. Meteor. Soc. Japan*, **73**, 795–809.

Waliser, D. E., and Coauthors, 2003: AGCM simulations of intraseasonal variability associated with the Asian summer monsoon. *Climate Dyn.*, **21**, 423–446.

Wang, B., 2005: Theories. *Intraseasonal variability of the atmosphere-ocean climate system*, K. M. Lau and D. E. Waliser, Eds., Springer-Verlag, Heidelberg, Germany, 436pp.

Wang, B., and H. Rui, 1990: Synoptic Climatology of transient tropical intraseasonal convection anomalies—1975–1985. *Meteorology and Atmospheic Physics*, **44**, 43–61.

Wang, B., and X. H. Xu, 1997: Northern hemisphere summer monsoon singularities and climatological intraseasonal oscillation. *J. Climate*, **10**, 1071–1085.

Wang, B., and LinHo, 2002: Rainy season of the Asian-Pacific summer monsoon. *J. Climate*, **15**, 386–398.

Wang, B., and Coauthors, 2004: Design of a new dynamical core for global atmospheric models based on some efficient numerical methods. *Science in China* (A), **47**, 4–21.

Wu, R., and B. Wang, 2001: Multi-stage onset of the summer monsoon over the western North Pacific. *Climate Dyn.*, **17**, 277–289.

Xie, P., A. Yatagai, M. Chen, T. Hayasaka, Y. Fukushima, C. Liu, and S. Yang, 2007: A gauge-based analysis of daily precipitation over East Asia. *Journal of Hydrometeorology*, **8**, 607–627.

Yanai, M., C. Li, and Z. S. Song, 1992: Seasonal heating of the Tibetan Plateau and its effects on the evolution of the Asian summer monsoon. *J. Meteor. Soc. Japan*, **70**, 319–351.

Yang, H., and C. Y. Li, 2003: The relation between atmospheric intraseasonal oscillation and summer severe flood and drought in the Changjiang-Huaihe River basin. *Adv. Atmos. Sci.*, **20**, 540–553.

Yang, J., 2008: Climatological and transient intraseasonal oscillations in the East-Asia-Western North Pacific summer monsoon. Ph. D. dissertation, Insititute of Atmospheric Physics, Chinese Academy of Sciences, 106pp.

Yang, J., B. Wang, and B. Wang, 2008: Anticorrelated intensity change of the quasi-biweekly and 30–50 day oscillations over the South China Sea. *Geophys. Res. Lett.*, doi: 10. 1029/2008GL034449.

Yeh, T. C., S. Y. Tao and M. T. Li, 1958: On the sudden changes in the general circulation in June and October. *Acta Meteorologica Sinica*, **38**, 162–169.

Zhang, Q. Y., S. Y. Tao, and S. L. Zhang, 2003: The persistent heavy rainfall over the Yangtze River valley and its associations with the circulations over East Asia during summer. *Chinese J. Atmos. Sci.*, **27**, 1018–1030. (in Chinese)

Zhang, Y. S., T. Li, B. Wang, and G. X. Wu, 2002: Onset of the summer monsoon over the Indochina Peninsula: Climatology and interannual variations. *J. Climate*, **15**, 3206–3221.

Zhang, G. J., and N. A. McFarlane, 1995: Sensitivity of climate simulations to the parameterization of cumulus convection in the Canadian Climate Centre general circulation model. *Atmos.-Ocean*, **33**, 407–446.

Zhu, B. Z., and Z. S. Song, 1979: A review of research on the general circulation of East Asia. *Scientia Atmospherica Sinica*, **3**, 219–226. (in Chinese)